Chinese Chemical Letters 37 (2026) 111986

Contents lists available at ScienceDirect

Chinese Chemical Letters

journal homepage: www.elsevier.com/locate/cclet

Synergistic steric hindrance and multiple resonance effect for efficient TADF with narrowband emission and accelerated upconversion

Xilin Mu[a,b,d,1], Tong Wang[c,1], Deli Li[e,1], Denghui Liu[c], Jiahui Wang[d], Jiuyan Li[d], Shijian Su[c,*], Wei Li[a,b,*], Ziyi Ge[a,b,*]

[a] Ningbo Institute of Materials Technology and Engineering, Chinese Academy of Sciences, Ningbo 315201, China
[b] Center of Materials Science and Optoelectronics Engineering, University of Chinese Academy of Sciences, Beijing 100049, China
[c] State Key Laboratory of Luminescent Materials and Devices and Institute of Polymer Optoelectronic Materials and Devices, South China University of Technology, Guangzhou 510640, China
[d] Frontier Science Center for Smart Materials, College of Chemistry, Dalian University of Technology, Dalian 116024, China
[e] Institute for Smart Materials & Engineering, University of Jinan, Ji'nan 250022, China

ARTICLE INFO

Article history:
Received 26 May 2025
Revised 16 October 2025
Accepted 20 October 2025
Available online 21 October 2025

Keywords:
Spirofluorene
Multiple resonance
Narrowband emission
Organic light-emitting diodes
Steric hindrance
Thermally activated delayed fluorescence

ABSTRACT

Herein, we propose a synergistic regulation strategy that combines steric hindrance with the multiple resonance (MR) effect to design and synthesize a thermally activated delayed fluorescent (TADF) emitter, SF-PhDABNA. This is achieved by incorporating spirofluorene units and introducing *meta*-position phenyl linkages into the DABNA-1 core. As a result, SF-PhDABNA exhibits narrowband pure blue emission centered at 472 nm with a full width at half maximum (FWHM) of 23 nm. The unique steric hindrance structure of the material effectively suppresses π-π interaction, while maintaining a tightly ordered molecular arrangement through C–H···π and C–H···B weak intermolecular interactions. This special packing pattern ensures a high photoluminescence quantum yield (PLQY) of 86 % in the doped film. Moreover, the significant directionality of the transition dipole moment (TDM) further enhances the light output coupling efficiency, thereby significantly improving the electroluminescence (EL) performance. The corresponding TADF-sensitized (TSF) OLED based on SF-PhDABNA achieves a maximum external quantum efficiency (EQE_{max}) of 23.9 % with CIE coordinates of (0.121, 0.284).

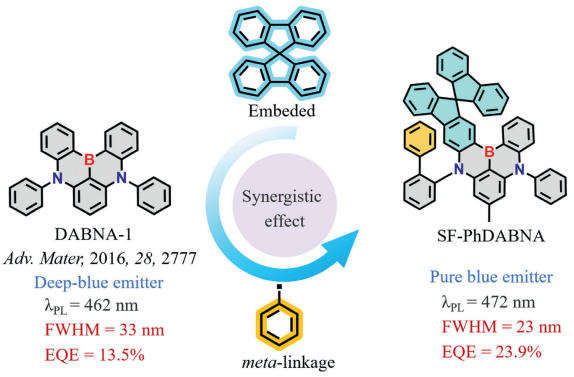
© 2026 Published by Elsevier B.V. on behalf of Chinese Chemical Society and Institute of Materia Medica, Chinese Academy of Medical Sciences.

Organic light-emitting diode (OLED) technology has achieved remarkable progress as a core display technology for the next generation [1]. With the advent of the 4K/8K ultra-high-definition (UHD) display era, there is a growing demand for displays with a wider color gamut. The BT.2020 standard, established by the International Telecommunication Union (ITU), requires display devices to be capable of covering an extended color gamut, thereby imposing strict requirements on the color purity of luminescent materials [2–4]. Although OLED technology offers numerous advantages, it is often limited by its broad emission spectrum, which leads to insufficient color purity and places it at a disadvantage compared to emerging materials such as quantum dots and perovskites [5–9]. Current strategies to address this limitation include using color filters and optical microcavities to narrow the electroluminescent (EL) spectra and enhance color purity [10].

In the realm of material development, conventional fluorescent materials are limited by spin-forbidden transitions, which prevent the utilization of triplet excitons, resulting in maximum external quantum efficiencies (EQEs) typically not exceeding 5 % [11,12]. Although phosphorescent materials can achieve high efficiency, they are hindered by issues such as the high cost of precious metals and environmental concerns. While capable of utilizing triplet excitons and tuning color emission [13,14]. Traditional D-A type thermally activated delayed fluorescence (TADF) materials suffer from inclusive emission spectra due to the intramolecular charge transfer (ICT) effect [15–18]. Therefore, achieving a balance between narrowband emission spectra and high efficiency remains a significant challenge. Common strategies to address this issue include using phosphorescent or TADF materials as sensitizing hosts, or incorporating multiple resonance (MR) effect from a molecular engineering perspective to enhance EL properties. In 2014, Adachi *et al.* proposed the use of TADF materials to sensitize conventional fluorescent materials, achieving a maximum external quantum efficiency (EQEmax) of 13.4 % to 18 %, thus overcoming the previous limitation of 5 % EQE [19]. In 2016, Hatakeyama *et al.* reported the

* Corresponding authors.
E-mail addresses: mssjsu@scut.edu.cn (S. Su), liwei1987@nimte.ac.cn (W. Li), geziyi@nimte.ac.cn (Z. Ge).
[1] These authors contributed equally to this work.

https://doi.org/10.1016/j.cclet.2025.111986
1001-8417/© 2026 Published by Elsevier B.V. on behalf of Chinese Chemical Society and Institute of Materia Medica, Chinese Academy of Medical Sciences.



Scheme 1. Molecular design strategy and chemical structures of the emitters.

successful embedding of boron (B) and nitrogen (N) atoms into a rigid polycyclic aromatic hydrocarbon (PAH) framework, effectively achieving the separation and localization of frontier molecular orbitals (FMOs), resulting in narrowband emission [20–24]. Despite its excellent performance, this type of material suffers from issues such as fluorescence quenching at high concentrations and significant energy gaps due to its inherent planar configuration. These factors often lead to slow reverse intersystem crossing (RISC) processes and triplet exciton annihilation, which are detrimental to solid-state luminescence [25–31]. The classical molecule DABNA-1, as reported, exemplifies these issues. Furthermore, these materials typically face challenges such as complex synthesis processes, the use of hazardous lithium reagents, and unstable yields. Therefore, developing simple and efficient and straightforward molecular design strategies to enhance triplet exciton utilization without compromising color purity has become a key challenge.

Herein, we employed a molecular engineering strategy to optimize the structure of the DABNA-1 core by introducing bulky spirofluorene units [32] and *meta*-substituted phenyl modifications, resulting in the successful synthesis of a novel narrowband luminescent material, SF-PhDABNA (Scheme 1). This molecular design enables precise control over molecular configuration and intermolecular interactions, significantly enhancing the material's horizontal orientation and solid-state luminescence efficiency while maintaining its narrowband emission characteristics. Specifically, SF-PhDABNA exhibits pure blue emission in toluene solution, with an emission peak at 472 nm and a FWHM of 23 nm. Compared to DABNA-1, the molecule undergoes a red shift, but the color purity is not compromised; on the contrary, it achieves narrowband emission, primarily attributed to the intramolecular charge transfer (ICT) effect. Additionally, the strong rigidity of the molecular configuration effectively alleviates vibrational relaxation. Notably, the doped film of SF-PhDABNA demonstrates a relatively high photoluminescence quantum yield (PLQY) of 86% under vacuum conditions, along with a radiative decay rate as high as 10^7 s^{-1} and a significantly large reverse intersystem crossing rate of 10^5 s^{-1}. The transient PL spectra exhibit a biexponential decay characteristic, confirming their TADF properties. Furthermore, the molecular stacking arrangement plays a crucial role in solid-state emission. The SF-PhDABNA molecule exhibits a unique stacking behavior. On one hand, the bulky peripheral substituents effectively prevent π-π stacking, avoiding quenching of the MR chromophore due to aggregation. On the other hand, intermolecular C–H···π and C–H···B interactions promote the formation of a tightly ordered molecular arrangement, which further suppresses vibrational relaxation of the electronic structure and enhances radiative decay. The transition dipole moment (TDM) orientation indicates a preferential horizontal alignment of the SF-PhDABNA molecule in the doped film, favoring improved light coupling efficiency [33]. Based on these

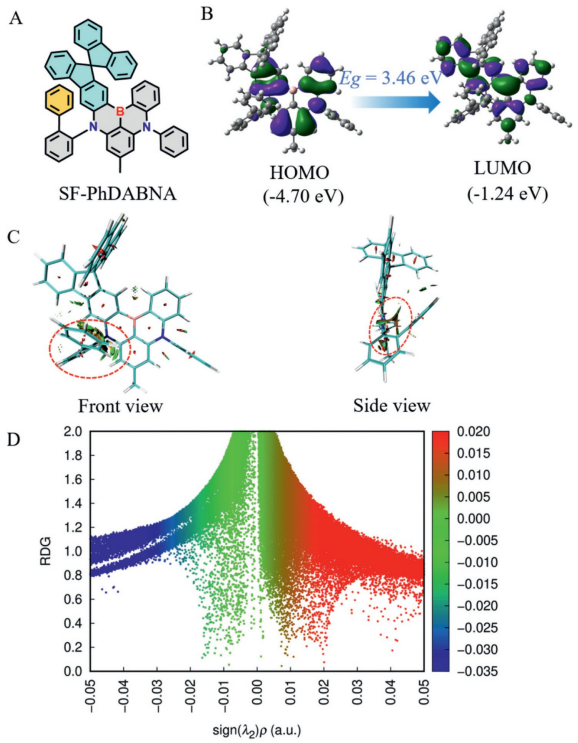


Fig. 1. (A) Molecular structure of SF-PhDABNA. (B) Frontier molecular orbital (FMO) distributions. The distribution of RDG isosurfaces (C) with the scatter plot of RDG *versus* sign(λ_2)ρ (D).

outstanding photophysical properties, we first fabricated a binary-doped OLED device using SF-PhDABNA, achieving an EQE maximum of 20.5% with pure blue narrowband emission. To fully harness the triplet excitons, a TADF-sensitized device (TSF-OLED) was constructed using m-MDBA-DI as the sensitizing host, resulting in EQE of 23.9% and CIE coordinates (0.121, 0.284), with a noticeable improvement in efficiency roll-off compared to the binary-doped device.

The synthesis procedure for SF-PhDABNA is detailed in Scheme S1 (Supporting information). The pivotal one-pot boronation cycloaddition step was adapted from the methyl-positioning method [34,35]. The target molecule SF-PhDABNA has undergone high-vacuum gradient sublimation purification to ensure high purity. ^{1}H NMR, ^{13}C NMR, high-resolution mass spectrometry, and single-crystal X-ray diffraction analysis have been used to determine its structure. Thermal properties of SF-PhDABNA are evaluated using differential scanning calorimetry (DSC) and thermogravimetric analysis (TGA) (Fig. S1 and Table S1 in Supporting information). The decomposition temperature (T_d, corresponding to 5% weight loss) of SF-PhDABNA is 477 °C, indicating its superior thermal stability. SF-PhDABNA exhibits a glass transition temperature (T_g) of 193 °C. These excellent thermal properties of SF-PhDABNA make it suitable for vacuum deposition. Electrochemical properties of SF-PhDABNA are investigated by cyclic voltammetry (CV) measurements (Fig. S2 and Table S1 in Supporting information). The highest occupied molecular orbital (HOMO) energy level (E_{HOMO}) of SF-PhDABNA is determined to be −5.20 eV. According to the UV-vis absorption spectra of SF-PhDABNA, the optical energy gap (E_g) is calculated to be 2.63 eV. The lowest unoccupied molecular orbital (LUMO) energy level (E_{LUMO}) of SF-PhDABNA is calculated using the formula $E_{LUMO} = E_{HOMO} + E_g$, which is determined as −2.57 eV.

The structure of the target molecule was optimized through density functional theory (DFT) calculations. As depicted in Fig. 1A, the spirofluorene unit adopts an orthogonal conformation, which

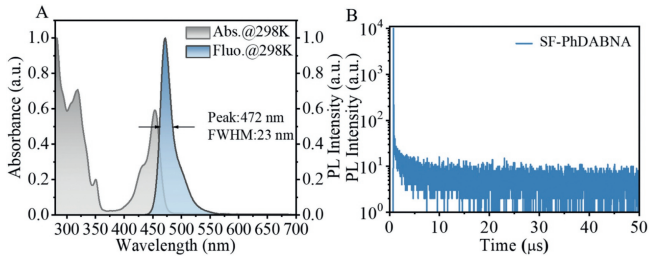


Fig. 2. (A) UV-vis absorption and PL spectra of SF-PhDABNA in dilute toluene solution. (B) Transient PL decay curves of SF-PhDABNA in doped films.

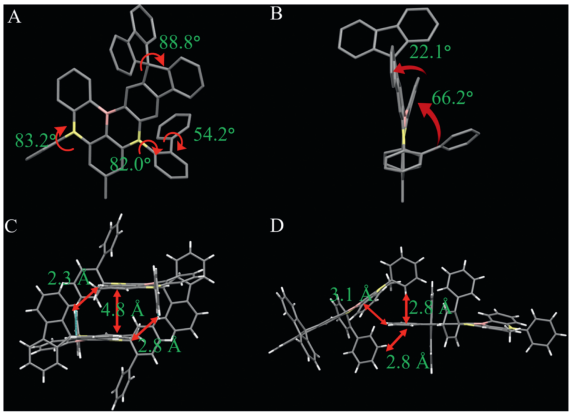


Fig. 3. (A) Front view and (B) side view of SF-PhDABNA. (C, D) Intermolecular packing modes of SF-PhDABNA in its representative dimers (CCDC: 2389656).

significantly inhibits molecular aggregation and prevents fluorescence quenching [32,36–38]. The pendant phenyl group is connected to one side of the spirofluorene unit *via* a *meta*-positioned linkage to the MR-BN backbone, forming a highly twisted structure [39]. This configuration further enhances the rigidity of the molecule and suppresses non-radiative decay. FMOs analysis reveals that the HOMO is primarily delocalized on the parent core DABNA-1 (−4.75 eV), with a closely matched energy level of −4.70 eV. The LUMO is distributed across the MR-BN backbone and partially delocalized onto the fluorene unit, with an energy level of −1.24 eV, which is deeper than that of DABNA-1′s LUMO (−1.09 eV) (Fig. 1B and Fig. S3 in Supporting information). This is attributed to the stabilization effect from the extended conjugation length. Moreover, the effective extension of the FMOs promotes the long-range charge transfer (LRCT) effect, potentially leading to red-shifted emission compared to DABNA-1. The natural transition orbital (NTO) exhibits MR-dominated characteristics, and the delocalization of electrons in the S_1 state is higher for holes, introducing a distinct charge transfer state to the MR system (Fig. S4 in Supporting information). Additionally, SF-PhDABNA exhibits a significantly higher oscillator strength ($f \sim 0.234$), indicating an efficient S_1-S_0 radiative transition process. Furthermore, the calculated energy levels for the S_1 and T_1 states are 2.69 and 2.52 eV, respectively, with singlet-triplet energy splitting ($\Delta E_{ST} \sim 0.17$ eV). A reduced density gradient (RDG) analysis was performed to investigate the intramolecular steric hindrance (Figs. 1C and D) [40]. The isosurface is colored on a blue-green-red scale based on sign(λ_2)ρ with a range from −0.05 to 0.05. The blue region represents the attractive interaction, while the red area indicates the repulsive effect. A green region is observed between the twisted phenyl group and the MR-BN backbone, signifying a relatively strong interaction between them. The significant spatial steric hindrance between these segments also leads to more compact molecular packing, promoting radiative transitions, narrowband emission, and high photoelectric efficiency [41–43].

To investigate the target molecule's photophysical properties, we measured its ultraviolet-visible (UV-vis) absorption and photoluminescence (PL) spectra in a dilute toluene solution (Fig. 2A and Table S1). In the UV-vis absorption spectra at 454 nm, a narrow and sharp absorption peak with MR characteristics was observed. In the PL spectra, SF-PhDABNA exhibits an emission peak at 472 nm, indicating pure blue fluorescence. Compared to DABNA-1, the narrowband emission undergoes a 10 nm redshift, which is attributed to the extended intramolecular conjugation (Fig. 2B) [44]. Notably, despite the slight red shift, the PL spectra of SF-PhDABNA did not broaden but instead exhibited a narrow FWHM of 23 nm. This suggests that the narrowband emission results from a synergistic effect from two factors: (1) the suppressed π-π stacking of the planar MR-BN framework, and (2) the introduction of twisted, sterically bulky substituent groups. Further solvent polarity-dependent studies revealed that the PL spectra exhibited a narrower FWHM of 18 nm in low-polarity environments but with a prominent shoulder. The energy levels of the S_1/T_1 excited states for SF-PhDABNA were determined to be 2.62 eV/2.48 eV, based on the onset values obtained from low fluorescence spectra and low-temperature phosphorescence spectra. SF-PhDABNA exhibited a small ΔE_{ST} of 0.14 eV (Fig. S8 and Table S1 in Supporting information), consistent with theoretical calculations. Compared to DABNA-1, SF-PhDABNA exhibits a smaller ΔE_{ST}, suggesting that the introduction of peripheral groups to the MR-BN framework facilitates the acceleration of the reverse intersystem crossing process, thereby enhancing triplet exciton utilization. As solvent polarity increased, the spectra red-shifted by 24 nm, the FWHM broadened, and the spectral profile became more structureless, exhibiting clear CT characteristics (Fig. S6 in Supporting information). These results demonstrate the modulation of photophysical properties by molecular structural modifications, particularly highlighting the contribution of the steric effect to the narrowband emission. To further investigate the actual photoluminescent characteristics of the device, we doped SF-PhDABNA at a concentration of 1 wt% and dispersed it in the mCBP host matrix. The PLQY and transient decay spectra were then measured. As shown in Fig. 2B, the transient PL spectrum exhibits a biexponential decay characteristic, encompassing both nanosecond-scale prompt fluorescence and microsecond-scale delayed fluorescence, thereby confirming its TADF properties. The results show that SF-PhDABNA possesses short prompt fluorescence lifetime ($\tau_p \sim 9.2$ ns) and delayed fluorescence lifetime ($\tau_d \sim 3.2$ μs), and achieves a substantial radiative transition rate ($\kappa_r \sim 7.2 \times 10^7$ s^{-1}), along with an impressive PLQY of 86% (Table S2 in Supporting information). Furthermore, it is noteworthy that such a short delayed fluorescence lifetime results in a reverse intersystem crossing rate exceeding 10^5 s^{-1}, which accelerates the triplet-state exciton upconversion process and effectively suppresses exciton annihilation. This also highlights that the spatially hindered groups in the molecular strategy of modifying the MR-BN framework have successfully addressed the issue of slow reverse intersystem crossing rates. These results are closely related to the molecular design and the tightly ordered arrangement between molecules.

To further explore the solid-state luminescence mechanism, the SF-PhDABNA single crystal was successfully cultivated using the slow evaporation method of a mixed solvent of chloroform/methanol. X-ray diffraction analysis was then performed (Fig. 3, Fig. S10 and Table S3 in Supporting information). The MR-BN skeleton exhibits slight deformation, with the peripheral spirofluorene units forming an approximately orthogonal configuration. Additionally, the *meta*-linked phenyl group forms a dihedral angle of about 66.2° with the MR-BN skeleton. This special configuration significantly enhances molecular rigidity and effectively inhibits

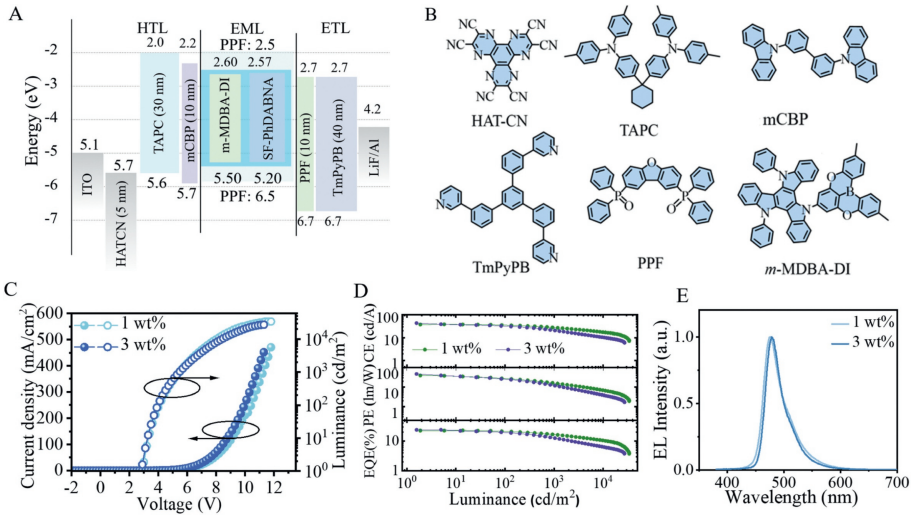


Fig. 4. (A) Device architecture and energy diagram. (B) Functional layer materials structures are used in these OLEDs. (C) Current density-voltage-luminance curves. (D) L-CE-PE-EQE curves of the device. (E) EL spectra (detected at the current density of 10 mA/cm^2).

Table 1
EL performance of the ternary TADF host sensitized OLEDs based on SF-PhDABNA, with doping concentrations of 1 wt% and 3 wt%.

Emitter	Dop. (wt%)	V_{on} (V) [a]	EQE (%) [b]			CE_{max} (cd/A) [c]	L_{max} (cd/m^2) [d]	CIE (x, y) [e]	Peak (nm) [f]	FHWM (nm)
			Max.	@10^2 cd/m^2	@10^3 cd/m^2					
SF-PhDABNA	1	2.90	22.6	20.9	16.4	42.7	33938	(0.132, 0.249)	476	45
	3	2.85	23.9	19.2	12.5	43.6	27264	(0.121, 0.284)	478	36

[a] The turn-on voltage.
[b] The maximum external quantum efficiency.
[c] The maximum current efficiency.
[d] The maximum luminance.
[e] Commission Internationale de l'Eclairage.
[f] The peak emission of EL spectra.

exciton annihilation. Moreover, no π-π interaction (~4.8 Å) was observed in the molecular packing arrangement, which efficiently prevents the quenching of MR-BN chromophores due to aggregation. This can be attributed to the molecule's large significant steric hindrance effect. Simultaneously, the C–H···π and C–H···B interactions (2.3–3.1 Å) promote tight and orderly molecular packing, synergistically enhancing the radiative transition rate and ultimately leading to efficient luminescence.

Benefiting from the excellent solid-state luminescence and narrowband emission characteristics of SF-PhDABNA, we fabricated binary and ternary-doped devices to evaluate EL performance. SF-PhDABNA was doped at 1 wt%, 3 wt%, and 5 wt% concentrations into the DOBNA-oAr host matrix in the binary-doped devices to form the emissive layer. This host material possesses low polarity and a wide bandgap, effectively suppressing reverse energy transfer from the guest T_1 state and thereby confining the excitons within the emitter [45]. The relevant OLED device structure, energy level diagram, and chemical structure are described in Figs. S11A and B (Supporting information). It can be observed that at low doping concentrations, the emitter undergoes a slight redshift, while still maintaining a narrow FWHM, indicating that the steric hindrance strategy has somewhat suppressed the adverse effects of concentration quenching. Although steric hindrance reduces aggregation quenching by inhibiting π-π stacking, a high density of emitter accelerates the disordered diffusion of excitons between molecules, increasing exciton annihilation and thus lowering device efficiency. Through device optimization, a doping concentration of 3 wt% was found to be the optimal condition for the binary device. At this doping concentration, the OLED device based on SF-PhDABNA exhibits pure blue, narrowband emission at 472 nm (FWHM ~ 29 nm), with a slight broadening compared to the PL spectra in solution (Fig. S11 and Table S4 in Supporting information). Generally, when the TDM direction aligns with the plane of the material, high light output coupling can be achieved, potentially leading to a satisfactory EQE [46,47]. The calculated TDM of SF-PhDABNA suggests that its direction is primarily along the xy-plane, with minimal components along the z-axis due to twisted configuration (Fig. S5 in Supporting information). This characteristic suggests that the material may exhibit a preferential horizontal alignment in the film, which is beneficial for enhancing light extraction efficiency. Ultimately, the binary-doped device achieves EQE of 20.5% and CIE coordinates of (0.117, 0.192), outperforming the previously reported performance of DABNA-1. Notably, the characteristic peak of the host DOBNA-oAr observed at 430 nm in the EL spectra indicates that energy transfer between the host and guest has not yet been fully completed.

We constructed a ternary doped device using m-MDBA-DI as a TADF auxiliary host to further improve device performance (Fig. 4). As shown in Fig. S7 (Supporting information), the absorption spectra of SF-PhDABNA significantly overlap with the PL spectra of m-MDBA-DI, ensuring an effective Förster resonance energy transfer (FRET) process, which facilitates the utilization of triplet excitons through efficient energy transfer. The device exhibits a turn-on voltage of less than 3 V, with an emission peak at 478 nm, achieving an EQE of 23.9% (Table 1). Compared to the binary-doped device, the efficiency roll-off has been improved. However, the EL spectra show a noticeable broadening, with an FWHM of 36 nm, which may be attributed to the solid-state solvation effect induced by the highly polar m-MDBA-DI. This investigation into electroluminescent properties provides a molecular design strategy for a

pure blue emitter that simultaneously achieves narrowband emission and high efficiency.

In summary, we designed and synthesized a novel narrowband emission MR-TADF emitter, SF-PhDABNA, by modifying the MR-BN framework with spirofluorene and phenyl groups. Through spatial steric hindrance control, vibration relaxation was effectively suppressed, enabling highly efficient narrowband emission. The material exhibited pure blue emission at 472 nm in solution, with a FWHM of 23 nm. Using a molecular engineering approach, π-π stacking was successfully inhibited, thereby avoiding non-radiative losses, while maintaining compact and ordered molecular packing *via* intermolecular weak interactions, which facilitated efficient solid-state luminescence. The TSF-OLED device based on SF-PhDABNA achieved an EQEmax of 23.9% and CIE coordinates of (0.121, 0.284). The spatial steric hindrance and MR effect synergistic control strategy proposed herein provides a promising pathway for developing highly efficient blue emitters for OLEDs, which is critical for advancing next-generation UHD display technologies.

Declaration of competing interest

The authors declare that they have no known competing financial interests or personal relationships that could have appeared to influence the work reported in this paper.

CRediT authorship contribution statement

Xilin Mu: Writing – original draft, Software, Methodology, Data curation, Conceptualization. **Tong Wang:** Data curation. **Deli Li:** Software, Data curation. **Denghui Liu:** Software. **Jiahui Wang:** Software, Data curation. **Jiuyan Li:** Supervision. **Shijian Su:** Supervision. **Wei Li:** Writing – review & editing, Investigation. **Ziyi Ge:** Supervision, Funding acquisition.

Acknowledgments

This work is financially supported by the National Natural Science Foundation of China for Young Scholars (Class B) [Formerly National Science Fund for Distinguished Young Scholars] (No. 22522512), the National Natural Science Foundation of China (Nos. 22375212, U21A20331, 51773212, 81903743, and 52003088), the Hundred Talents Program of the Chinese Academy of Sciences (No. Y60707WR48), Zhejiang Province "Leading Goose" R&D Project (No. 2024C01261) and the Ningbo Key Scientific and Technological Project (Nos. 2022Z124, 2022Z119, 2022Z120).

Supplementary materials

Supplementary material associated with this article can be found, in the online version, at doi:10.1016/j.cclet.2025.111986.

References

[1] G. Hong, X. Gan, C. Leonhardt, et al., Adv. Mater. 33 (2021) 2005630.
[2] S.H. Ko, J. Rogers, Adv. Funct. Mater. 31 (2021) 2106546.
[3] D. Zhang, T. Huang, L. Duan, Adv. Mater. 32 (2020) e1902391.
[4] J.M. Ha, H.B. Shin, J.F. Joung, et al., ACS Appl. Mater. Interfaces 13 (2021) 26227–26236.
[5] Z. Yang, Z. Mao, Z. Xie, et al., Chem. Soc. Rev. 46 (2017) 915–1016.
[6] A.D. Broadbent, Color Res. Appl. 29 (2004) 267–272.
[7] K. Lin, J. Xing, L.N. Quan, et al., Nature 562 (2018) 245–248.
[8] Y. Yang, Y. Zheng, W. Cao, et al., Nat. Photonics 9 (2015) 259–266.
[9] V.L. Colvin, M.C. Schlamp, A.P. Alivisatos, Nature 370 (1994) 354–357.
[10] M. Fröbel, F. Fries, T. Schwab, et al., Sci. Rep. 8 (2018) 9684.
[11] Y. Xu, P. Xu, D. Hu, et al., Chem. Soc. Rev. 50 (2021) 1030–1069.
[12] Y. Chi, P.T. Chou, Chem. Soc. Rev. 39 (2010) 638–655.
[13] B. Minaev, G. Baryshnikov, H. Agren, Phys. Chem. Chem. Phys. 16 (2014) 1719–1758.
[14] T. Fleetham, G. Li, J. Li, Adv. Mater. 29 (2017) 1601861.
[15] H. Uoyama, K. Goushi, K. Shizu, et al., Nature 492 (2012) 234–238.
[16] Y. Chi, P.T. Chou, Chem. Soc. Rev. 39 (2010) 638–655.
[17] B. Minaev, G. Baryshnikov, H. Agren, Phys. Chem. Chem. Phys. 16 (2014) 1719–1758.
[18] T. Fleetham, G. Li, J. Li, Adv. Mater. 29 (2017) 1601861.
[19] H. Nakanotani, T. Higuchi, T. Furukawa, et al., Nat. Commun. 5 (2014) 4016.
[20] T. Hatakeyama, K. Shiren, K. Nakajima, et al., Adv. Mater. 28 (2016) 2777–2781.
[21] X. Liang, Z. Yan, H. Han, et al., Angew. Chem. Int. Ed. 130 (2018) 11486–11490.
[22] L. Yang, X. Xin, R. You, et al., Chem. Sci. 12 (2021) 9408–9412.
[23] X. Cai, Y. Pan, C. Li, et al., Angew. Chem. Int. Ed. 63 (2024) e202408522.
[24] J. Han, Y. Chen, N. Li, et al., Aggregate 3 (2022) e182.
[25] M. Yang, I.S. Park, T. Yasuda, J. Am. Chem. Soc. 142 (2020) 19468–19472.
[26] Y. Wang, Y. Tian, Y. Gao, et al., J. Phys. Chem. Lett. 14 (2023) 9665–9676.
[27] D. Zhang, T. Huang, L. Duan, Adv. Mater. 32 (2020) e1902391.
[28] H.J. Kim, T. Yasuda, Adv. Opt. Mater. 10 (2022) 2201714.
[29] X. Cai, Y. Pu, C. Li, et al., Angew. Chem. Int. Ed. 62 (2023) e202304104.
[30] Y. Zhang, J. Wei, D. Zhang, et al., Angew. Chem. Int. Ed. 61 (2022) e202113206.
[31] X. Yan, Z. Li, Q. Wang, et al., J. Mater. Chem. C 10 (2022) 15408–15415.
[32] L. Wu, C. Liu, D. Liu, et al., Angew. Chem. Int. Ed 64 (2025) e202504723.
[33] H. Lee, R. Braveenth, S. Muruganantham, et al., Nat. Commun. 14 (2023) 419.
[34] L. Wu, Z. Huang, J. Miao, et al., Angew. Chem. Int. Ed. 63 (2024) e202402020.
[35] T. Feng, X. Nie, D. Liu, et al., Angew. Chem. Int. Ed. 64 (2025) e202415113.
[36] H. Cheng, J. Lan, Y. Yang, et al., Mater. Horiz. 11 (2024) 4674–4680.
[37] L. Wu, X. Mu, D. Liu, et al., Angew. Chem. Int. Ed. 63 (2024) e202409580.
[38] S.Q. Song, X. Han, Z.Z. Huo, et al., Sci. China Chem. 67 (2024) 2257–2264.
[39] X. Mu, D. Li, D. Liu, et al., Adv. Opt. Mater. 12 (2024) 2401735.
[40] T. Lu, F. Chen, J. Comput. Chem. 33 (2012) 580–592.
[41] Q. Li, H. Zhao, M. Li, et al., Angew. Chem. Int. Ed. 64 (2025) e202506654.
[42] P. Li, Z. Chen, M.Y. Leung, et al., J. Am. Chem. Soc. 147 (2025) 12092–12104.
[43] J. Zhang, D. Li, W. Li, et al., Sci. China Chem. 67 (2024) 1270–1276.
[44] X. Mu, L. Wu, Z. Li, et al., Small 21 (2025) 2411961.
[45] Y. Kondo, K. Yoshiura, S. Kitera, et al., Nat. Photonics 13 (2019) 678–682.
[46] F. Tenopala-Carmona, O.S. Lee, E. Crovini, et al., Adv. Mater. 33 (2021) 2100677.
[47] J.M. Dos Santos, D. Hall, B. Basumatary, M. Bryden, et al., Chem. Rev. 124 (2024) 13736–14110.